J. Membrane Biol. 82, 67–82 (1984)

The Journal of
Membrane Biology

General Method for the Derivation and Numerical Solution of Epithelial Transport Models

Richard Latta*, Chris Clausen, and Leon C. Moore
Department of Physiology and Biophysics, Health Sciences Center, State University of New York at Stony Brook, Stony Brook, New York 11794

Summary. A general method is presented for the formulation and numerical evaluation of mathematical models describing epithelial transport. The method is based on the principles of conservation of mass, and maintenance of electroneutrality within the cells and bathing solutions. It is therefore independent of the specific membrane transport mechanisms, and can be used to evaluate different models describing arbitrary transport processes (including passive, active and cotransport processes). Detailed numerical methods are presented that allow computation of steady-state and transient responses under open-circuit, current-clamp and voltage-clamp conditions, using a general-purpose laboratory minicomputer. To evaluate the utility of this approach, a specific model is presented that is consistent with the Koefoed-Johnson and Ussing hypothesis of sodium transport in tight epithelia (*Acta Physiol. Scand.* **42**:298–308, 1958). This model considers passive transport of an arbitrary number of permeant solutes, active transport of sodium and potassium, and osmotically induced water transport across the apical and basolateral membranes. Results of the model are compared to published experimental measurements in rabbit urinary bladder epithelium.

Key Words Epithelial transport · mathematical models · cell volume · intracellular composition · sodium transport · Ussing model · tight epithelia · mammalian urinary bladder

Introduction

Epithelial transport involves the complex interaction of many specific transport processes located within the three different epithelial membranes: the apical, basolateral and junctional membranes. These transport mechanisms may be relatively simple, like electrodiffusion, or highly complex, such as cotransport or active transport. In addition, transepithelial transport of one substance will invariably be coupled to the transport of other substances, either directly owing to specific cotransport mechanisms, or indirectly because of secondary changes in electrochemical or osmotic driving forces. A fruitful experimental approach to the study of epithelial transport has been to measure transport phenomena, such as fluxes, membrane potentials, currents or conductances, under conditions where the observed behavior can be attributed to the transport of a limited number of solutes across a single membrane. This approach has yielded a wealth of information about specific transport mechanisms for many solutes. However, the very nature of this experimental strategy makes it difficult to reconstruct a quantitative, unified description of transport across an intact epithelium from collections of single membrane data, especially when a number of different experimental methods are employed. This problem becomes increasingly severe when considering a complex epithelium where many substances may be transported simultaneously, where varying intracellular and bathing solution composition alters membrane transport parameters, where intracellular and membrane reactions may lead to the production or conversion of transported substances, and where cell and lateral space geometry may be important determinants of net transport.

A specific example where such complications have arisen, and which will be discussed in detail in this paper, is Na^+ transport in rabbit urinary bladder, an aldosterone-stimulated tight epithelium that reabsorbs Na^+ from mucosa to serosa. The mechanism is thought to be described in part by the Koefoed-Johnson and Ussing (1958) hypothesis. The apical, basolateral and junctional membrane characteristics have been measured: the apical membrane is permeable only to Na^+ and K^+; the basolateral membrane possesses a Na,K-ATPase (sodium pump) and is permeable mainly to K^+ and Cl^-; the junctions are nearly impermeable. Intracel-

* *Current address:* School of Medicine, Medical College of Pennsylvania, Philadelphia, Pennsylvania.

lular ionic composition measurements have shown that Na^+ levels are virtually independent of transport rate, an intriguing observation since Na,K-ATPase activity is known to be regulated in part by intracellular Na^+. Analysis of this observation clearly requires integration of the transport events occurring at each of the membranes. Another question of interest is the relevance of transport-parameter measurements that could only be made under grossly nonphysiological conditions. For example, sodium-pump kinetics were studied under conditions of high extracellular K^+ activity and in the presence of channel-forming antibiotics to eliminate functionally the apical membrane as a barrier to ion flow. Resolution of this question requires a means to determine if such parameter measurements are consistent with normal epithelial function.

For these kinds of problems, the formulation of a mathematical model is appropriate and useful since it provides a systematic means to integrate the separate membrane transport mechanisms into a comprehensive description of the epithelial system. When used in conjunction with experimental studies, such mathematical models have proven to be useful in the design of experiments and the estimation of transport parameters. Moreover, because a properly formulated mathematical model is an explicit, unambiguous statement of a complex hypothesis, comparison of the model predictions with known behavior of an intact epithelium can provide valuable insight into the consistency of experimental data and the adequacy of a hypothesis to explain quantitatively epithelial behavior. However, this approach has not been widely used because of the complexities inherent to epithelia, and the lack of a general method to compute potential differences, and hence electrochemical gradients, across membranes possessing arbitrary transport characteristics.

In this paper we first discuss three topics which are applicable to the development of epithelial transport models in general:

1. We present a procedure for the derivation of mathematical models of epithelial transport based on fundamental considerations of conservation of mass and the imposition of appropriate electroneutrality constraints. The procedure is applicable to many different epithelia, since each differs only in the form of the specific auxiliary equations describing the different membrane solute fluxes (e.g., electrodiffusion, active transport, cotransport), water fluxes (e.g., osmotic, hydrostatic), and boundary conditions (e.g., unstirred layers, restricted extracellular spaces).

2. We develop a numerical method for the solution of the set of differential equations that constitute a mathematical model of an epithelium. The method calculates the steady-state and transient responses under simulated open-circuit, current-clamp or voltage-clamp conditions.

3. We discuss ways to evaluate the models efficiently using a laboratory computer of modest capability.

We subsequently illustrate the application of these general methods with a specific example:

1. We derive and solve a specific model describing sodium transport across a tight epithelium based on the Koefoed-Johnson and Ussing (1958) hypothesis. This model is similar to that developed by Lew, Ferreira and Moura (1979) and used subsequently by Civan and Bookman (1982). It is an extension of these investigators' work in that it permits consideration of an arbitrary number of solutes, allows each of the solutes to possess arbitrary valence, and specifically considers osmotically induced water transport across the apical and basolateral membranes.

2. We evaluate the model by comparing its predictions (steady-state and transient behavior) with an extensive set of experimental observations of mammalian urinary bladder.

Theoretical Analysis

The goal of this analysis is to obtain a general set of differential equations (state equations) that describe cell volume and intracellular solute concentrations as time-variant functions of the transmembrane mass fluxes and cellular geometry. Subsequently, relationships arising from constraints of electroneutrality are presented. Finally, auxiliary equations are specified that describe the solute and water fluxes across each of the epithelial membranes as functions of the membrane electrochemical gradients, membrane transport parameters and kinetic descriptions of active transport and cotransport processes.

The general analysis starts with the description of a single representative cell within the epithelium. Assuming that most cells behave in a similar fashion, the analysis can easily be extended to represent properties of a unit area of epithelium by scaling appropriately by the cell density. The bathing solutions are assumed to be infinite in volume, thereby implying that transepithelial transport does not alter bath composition. This assumption could be relaxed with no loss of generality regarding the numerical approach to the evaluation of the model simply by including appropriate state equations describing mass balance in the baths. It is also assumed that the cell and the mucosal and serosal bathing solu-

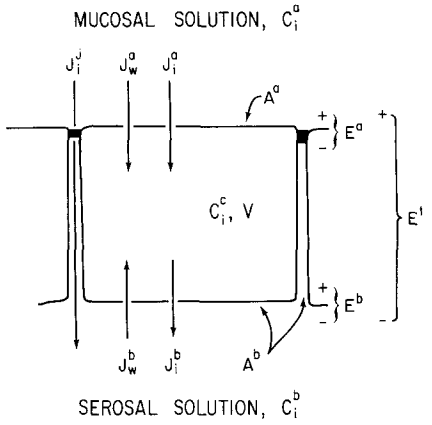

Fig. 1. Schematic representation of the general epithelial model. Consult the text for definition of the symbols. The straight arrows denote direction of positive solute and water fluxes. Orientation of membrane potentials are denoted by + and − (e.g., a positive value for E^t means that the mucosal solution is positive with respect to the serosal solution)

tions are well stirred, hence unstirred layer effects are ignored. This assumption could also be relaxed, but this would require additional state equations which include geometrical independent variables (e.g., distance), thereby resulting in a set of partial differential equations. The numerical solution of this kind of initial boundary-value problem is possible with a straightforward extension of the methods presented below, but it is a subject beyond the scope of this paper.

A schematic representation of the general model is illustrated in Fig. 1, which shows the orientation of the solute and water fluxes. The definition of the symbols and the detailed derivation of the equations are presented below.

The State Equations

Conservation of cellular water yields a differential equation describing cell volume V (cm^3) as a function of the water fluxes:

$$dV/dt = A^a J_w^a + A^b J_w^b. \quad (1)$$

A^a and A^b (cm^2) are the apical and basolateral membrane areas, respectively. J_w^a and J_w^b [cm^3/(sec cm^2)] are the respective apical and basolateral water fluxes. A positive value for water flux is defined as an influx of water. Implicit in Eq. (1) is that solute partial molar volumes are negligible.

A similar conservation analysis yields a differential equation for each intracellular solute, the concentration of which is dependent upon apical and basolateral solute fluxes, as well as concentrating and diluting effects caused by water movement:

$$VdC_i^c/dt = A^a J_i^a - A^b J_i^b - C_i^c(A^a J_w^a + A^b J_w^b). \quad (2)$$

Subscript i identifies each solute species. C_i^c (mol/cm^3) is the intracellular concentration, and J_i^a and J_i^b [mol/(sec cm^2)] refer to the solute fluxes across the apical and basolateral membranes, respectively. A positive flux across the apical membrane is an influx, whereas a positive flux across the basolateral membrane is an efflux.

The model is evaluated by assuming initial conditions for the state variables and integrating Eqs. (1) and (2) over time to compute $C_i^c(t)$ and $V(t)$. The mass fluxes are defined with the auxiliary equations presented below. In all cases, the solution is subject to additional electroneutrality constraints appropriate for different experimental conditions as explained below.

Coupling of Equations and the Calculation of Membrane Potentials

The differential equations presented above are inherently coupled to each other. The apical and basolateral fluxes of each solute are influenced by the common intracellular concentration C_i^c, and the fluxes of all solutes can interact indirectly whenever intracellular osmolarity is altered due to changes of the flux of a single solute. However, when considering fluxes of charged solutes with valence z_i, these interactions are not sufficient to guarantee that the cell remains electrically neutral $\left(\text{i.e., } \sum_i z_i C_i^c = 0\right)$. Hence a constraint must be imposed in order to prevent net charge flux into or out of the cell, which otherwise would result in a violation of electroneutrality.

A slight violation of electroneutrality does, in fact, occur because of charge separation due to the polarization of membrane capacitances. However, calculations for typical epithelial cells indicate that this results in only negligible changes in the actual intracellular ionic concentrations. Hence, we will ignore this effect.

Apical and basolateral charge fluxes can be represented electrically as membrane currents:

$$I^a = FA^a \sum_i z_i J_i^a;\ I^b = FA^b \sum_i z_i J_i^b \quad (3)$$

where F is Faraday's constant. The constraint that ensures cellular electroneutrality is simply that the current entering the cell across the apical mem-

brane must equal the current leaving the cell via the basolateral membrane. Hence at all times,

$$I^a = I^b. \tag{4}$$

Additional constraints, notably maintenance of mucosal and serosal bath electroneutrality, will be imposed in order to simulate different experimental situations, such as open-circuit, current-clamp and voltage-clamp experimental conditions (*see* Methods).

The flux of each electrolyte across a membrane is dependent on a common membrane potential, which effectively couples the ionic flux equations. The problem, therefore, is to devise a computational scheme (*see* Methods) to solve for the unique membrane potential across each respective membrane such that the resulting charge fluxes are consistent with Eq. (4). Note that the use of an ionic equilibrium potential is not appropriate since it is specific to the mechanism of electrolyte transport (e.g., constant-field assumption), and since the distribution of electrolytes across each membrane will generally not be at equilibrium.

The transepithelial and basolateral membrane potentials (E^t and E^b, respectively) are defined with respect to a reference potential on the serosal side (*see* Fig. 1). E^t is defined also to be the sum of the two membrane potentials (i.e., $E^t = E^a + E^b$), hence E^a is defined with respect to inside the cell. For the ionic flux equations (*see below*), it is convenient to consider normalized (unitless) membrane potentials, U^a, U^b and U^t given by:

$$U^a = E^aF/RT;\ U^b = E^bF/RT;\ U^t = E^tF/RT \tag{5}$$

where R is the gas constant, and T is the absolute temperature.

Auxiliary Equations for a Na^+-transport Model

Since the basic principles of mass balance and maintenance of electroneutrality are central to epithelial transport in general, the state equations and electroneutrality constraints discussed above are therefore applicable to any specific epithelial transport model. A general method for the solution of the state equations (Eqs. 1 and 2), subject to the electroneutrality constraints, is presented in the Methods section. All that remains is to specify a set of specific auxiliary equations describing the membrane solute and water fluxes in a specific epithelium. The actual number of auxiliary equations, and their functional forms, depends on the specific membrane transport processes present. Hence, the auxiliary equations will be different for different epithelia.

We now present a minimal set of auxiliary flux equations that describe a specific model of the Koefoed-Johnson and Ussing (1958) hypothesis of epithelial Na^+ transport. Keep in mind that additional equations and terms could be added to represent additional transport processes. In the discussions that follow, we will refer to this specific model as the Na^+ model.

Our formulation of the Na^+ model, as well as the actual computer program, permits an arbitrary number of solutes, but for sake of simplicity we will consider only six different species: Na^+, K^+, Cl^-, $X_1^{n_1}$, $X_2^{n_2}$ and $X_3^{n_3}$. Recall that subscript i refers to each of these species. X_1, X_2 and X_3 represent three arbitrary, possibly heterogeneous, solutes. These are used to impose initial charge and osmotic balance. They can also be used subsequently for altering cell and/or bathing solution osmolarity, and to provide for solute substitutions. The valences n_1, n_2 and n_3 can take on arbitrary values, including zero for the representation of nonelectrolytes, and nonintegral values for the representation of heterogeneous impermeant species.

Water Fluxes

We consider only osmotically induced water flux across the apical and basolateral membranes (the paracellular pathway is assumed to be impermeable to water), and assume that the cell membranes are incapable of supporting hydrostatic gradients. These fluxes are given by

$$J_w^a = L_p^a RT \sum_i \sigma_i^a (C_i^c - C_i^a); \tag{6}$$

$$J_w^b = L_p^b RT \sum_i \sigma_i^b (C_i^c - C_i^b).$$

L_p^a and L_p^b [cm³/(dyne sec)] are the hydraulic conductances of the apical and basolateral membranes, respectively. σ_i^a and σ_i^b denote the respective solute reflection coefficients. C_i^a and C_i^b (mol/cm³) are the solute concentrations in the mucosal and serosal baths, respectively.

Apical and Paracellular Solute Fluxes

Passive solute fluxes across all membranes in the Na^+ model are assumed to occur by electrodiffusion and to conform to the Goldman-Hodgkin-Katz constant-field flux equation (*cf.* Hodgkin & Katz, 1949).

Solute flux of the i'th species across the apical membrane is assumed to be entirely passive, thereby yielding

$$J_i^a = P_i^a z_i U^a \frac{C_i^a - C_i^c \exp(-z_i U^a)}{1 - \exp(-z_i U^a)}. \quad (7)$$

P_i^a (cm/sec) are the apical membrane permeabilities. For unchanged solutes or zero transmembrane potential, the appropriate limiting case of Eq. (7) (and the other similar equations below) is used to describe simple diffusion.

Similarly, under conditions where the junctional permeability to the solutes is finite (i.e., leaky or moderately tight epithelium), the paracellular flux for the i'th species is also assumed to be passive and is given by

$$J_i^j = P_i^j z_i U^t \frac{C_i^a - C_i^b \exp(-z_i U^t)}{1 - \exp(-z_i U^t)}. \quad (8)$$

P_i^j (cm/sec) represents the solute permeabilities of the paracellular pathway determined by the combined properties of the tight junctions and lateral spaces.

Basolateral Solute Fluxes

Solute movement across the basolateral membrane is also assumed to occur passively by electrodiffusion, and by active transport via the sodium pump:

$$J_i^b = P_i^b z_i U^b \frac{C_i^c - C_i^b \exp(-z_i U^b)}{1 - \exp(-z_i U^b)} + J_i^p, \quad (9)$$

where P_i^b (cm/sec) are the basolateral membrane solute permeabilities, and J_i^p [mol/(sec cm^2)] are the fluxes attributable to the sodium pump. J_i^p refers only to an active Na^+ efflux J_{Na}^p, and a K^+ influx J_K^p.

Lewis and Wills (1981) measured the short-circuit current as a function of the serosal K^+ concentration and the intracellular Na^+ activity and found that the current could be expressed as

$$I^p = \frac{I_{max}}{[1 + (K_{Na}/C_{Na}^c)^{n_{Na}}][1 + (K_K/C_K^b)^{n_K}]}. \quad (10)$$

This expression is based on a saturable kinetic model with highly competitive binding (Nelson & Blaustein, 1980), and implies a Na^+-to-K^+ coupling ratio of n_{Na}/n_K (i.e., n_{Na} intracellular sodium ions are translocated in exchange for n_K serosal potassium ions). I_{max} (A/cm^2) is the maximum observable pump current, K_{Na} and K_K (mol/cm^3) are the concentrations of intracellular Na^+ and serosal K^+ producing half-maximal pump currents, respectively. The corresponding Na^+ and K^+ fluxes can be expressed in terms of the pump current (Eq. 10) by:

$$J_{Na}^p = n_{Na} I^p/F; \; J_K^p = -n_K I^p/F. \quad (11)$$

Assumptions Inherent to the Na^+ Model

As stated earlier, we have purposely limited the formulation of the Na^+ model to a minimal set of equations consistent with the Koefoed-Johnson and Ussing (1958) notion of epithelial Na^+ transport. The structure of the Na^+ model and the numerical methods used in its solution are sufficiently general to permit ready expansion to include other transport processes and effects (such as those discussed below). All that needs to be done is to expand the appropriate flux equations (*see* Schultz, 1980, Ch. 4–6), or alter the parameters in a systematic way during the course of the integration; the method of computation remains unchanged.

Following is a list of the assumptions and simplifications of the Na^+ model:

1. The flux equations have not been justified from experimental data. Is it true experimentally that passive flux across each of the membrane obeys the Goldman-Hodgkin-Katz flux equations? Certainly this is the case observed in several different tissues, as determined by epithelial flux ratio measurements and current-voltage relationships (Thomson, Suzuki & Schultz, 1981), and bi-ionic potentials (Lewis, Wills & Eaton, 1978). However, other transport processes observable in sodium-transporting epithelia (e.g., active Cl^- pump, Cl^--HCO_3^- exchange processes, electroneutral NaCl transport processes, solute and solvent drag) are not included in this model.

2. Solute permeabilities are treated as invariant parameters. It has been observed that some membrane permeabilities are dependent on bathing solution composition, especially when considering Na^+ transport with dilute mucosal solutions (*cf.* Fuchs, Larsen & Lindemann, 1977). It has also been suggested that intracellular composition may affect solute permeabilities, especially in regard to a postulated negative feedback mechanism occurring at high transport rates that results in an inverse relationship between P_{Na}^a and C_{Na}^c (*cf.* Lewis, Eaton & Diamond, 1976; Turnheim, Frizzell & Schultz, 1978). These effects could easily be implemented by describing the permeabilities as functions of concentration using additional auxiliary equations.

3. The description of the Na,K-ATPase is empirical, hence the Na^+ model relies on the validity

of Eq. (10). However, Eq. (10) has been found to describe adequately the measured kinetics in Na^+-transporting epithelia (Lewis & Wills, 1981) and other tissues (Nelson & Blaustein, 1980). The formulation does not include limitations upon pumping rate imposed by cellular energetics (e.g., ATP availability), nor does it include limitations on the enzyme activity imposed by the Na^+ and K^+ electrochemical gradients across the basolateral membrane (Lewis & Wills, 1983). Note that in frog skin, the Na,K-ATPase is found to operate far from equilibrium and therefore changes in the activity of the pump are expected to be determined by its kinetic properties and not the overall thermodynamics of the system (Civan et al., 1983). It should also be noted that our description of the pump kinetics differs slightly from that used in the model of Lew et al. (1979), who used a noncooperative binding model.

4. Apical and basolateral membrane areas (A^a and A^b, respectively) are assumed to be constant. However, investigators have found that transport processes are often related to membrane area changes, notably in ADH-stimulated transport in toad bladder (Wade, Stetson & Lewis, 1981), proton secretion in turtle bladder (Gluck, Cannon & Al-Awqati, 1982), and HCl secretion in gastric mucosa (Forte, Machen & Forte, 1977). Transepithelial hydrostatic pressure gradients and simple distension of the epithelium have also been shown to alter membrane area (Lewis & de Moura, 1982).

5. The membrane fluxes, permeabilities, and hydraulic conductances used in the Na^+ model are normalized to the actual surface area of the apical and basolateral membranes. They can easily be represented as being normalized to unit epithelial surface area, as is common in experimental situations, simply by setting A^a and A^b to unity.

6. It is well known that the intracellular chemical concentrations of ionic species exceed their respective activities [measured, for example, with ion-selective microelectrodes; *see* Lewis & Wills (1978)]. In the Na^+ model, $C_i^{a,b,c}$ actually represent solute activities (not concentrations) since the respective fluxes and membrane potentials are assumed to be dependent on solute activity. This assumption implies that the respective solute activity coefficients and osmotic coefficients are equal.

Methods

Numerical Integration

Equations (1) and (2) can be integrated as a function of time using any appropriate algorithm for the numerical solution of ordinary differential equations (*see* Carnahan, Luther & Wilkes, 1969). We use a variable-step-size Runge-Kutta algorithm based on fifth- and sixth-order formulas. The actual routine is a variation of subroutine DVERK (Hull, Enright & Jackson, 1976)[1] that was modified to run utilizing single-precision arithmetic (7 to 8 significant digit accuracy). Computational accuracy was easily maintained at better than 0.1% throughout the integration.

The evaluation of the model involves integrating the state equations from an initial time (t_{initial}) to a final time (t_{final}) using small time increments (Δt). The detailed steps of the computation are shown as a flow chart in Fig. 2, and are as follows:

1. Transport parameters, initial conditions, t_{initial}, t_{final}, and Δt are specified, and the integration variable t is initialized to t_{initial}.
2. Membrane potentials are computed (*see below* and Figs. 3 and 4).
3. Solute and water fluxes are computed using the membrane potentials and the respective flux equations (Eqs. 6 through 9).
4. The state equations (Eqs. 1 and 2) are evaluated and are integrated to $t + \Delta t$.[2]
5. Additional variables are computed (e.g., membrane conductances, *see below*), and all results are saved off-line.
6. t is updated to $t + \Delta t$ and a comparison is made with t_{final}. If t_{final} has been reached, the computation ends. Otherwise, the program returns to step 2 to continue the integration.

Computation of Membrane Potentials

During each step in the integration, the membrane potentials must be computed subject to the constraint that the cell remains electroneutral. Eq. (4) must never be violated under any experimental condition, but the strategy used in computing the potentials depends on whether the computation is simulating a preparation that is voltage-clamped transepithelially, or one that is under current-clamp or open-circuit conditions.

Voltage-Clamp Case

Under voltage-clamp conditions, E^t is maintained at a constant value and the transepithelial current I^t is computed. The most common case is when E^t is maintained at zero, which results in the short-circuit current $I^t = I^{sc}$. For any potential E^t, I^t is comprised of the sum of two components: a transcellular current $I^a = I^b$, and a paracellular current I^j, which can be computed directly from Eq. (8) since

$$I^j = FA^a \sum_i z_i J_i^j. \tag{12}$$

The computation of the transcellular current, however, requires knowledge of either the apical potential E^a or the basolateral potential E^b, since if either of these two potentials can be determined, the other is easily determined from the fact that $E^t =$

[1] Available from the IMSL Library (International Mathematical and Statistical Libraries, Inc., Houston, Texas).

[2] DVERK actually subdivides Δt into smaller increments in order to maintain the specified accuracy. Hence, steps 2 through 4 are repeated using these smaller time intervals until $t + \Delta t$ is reached.

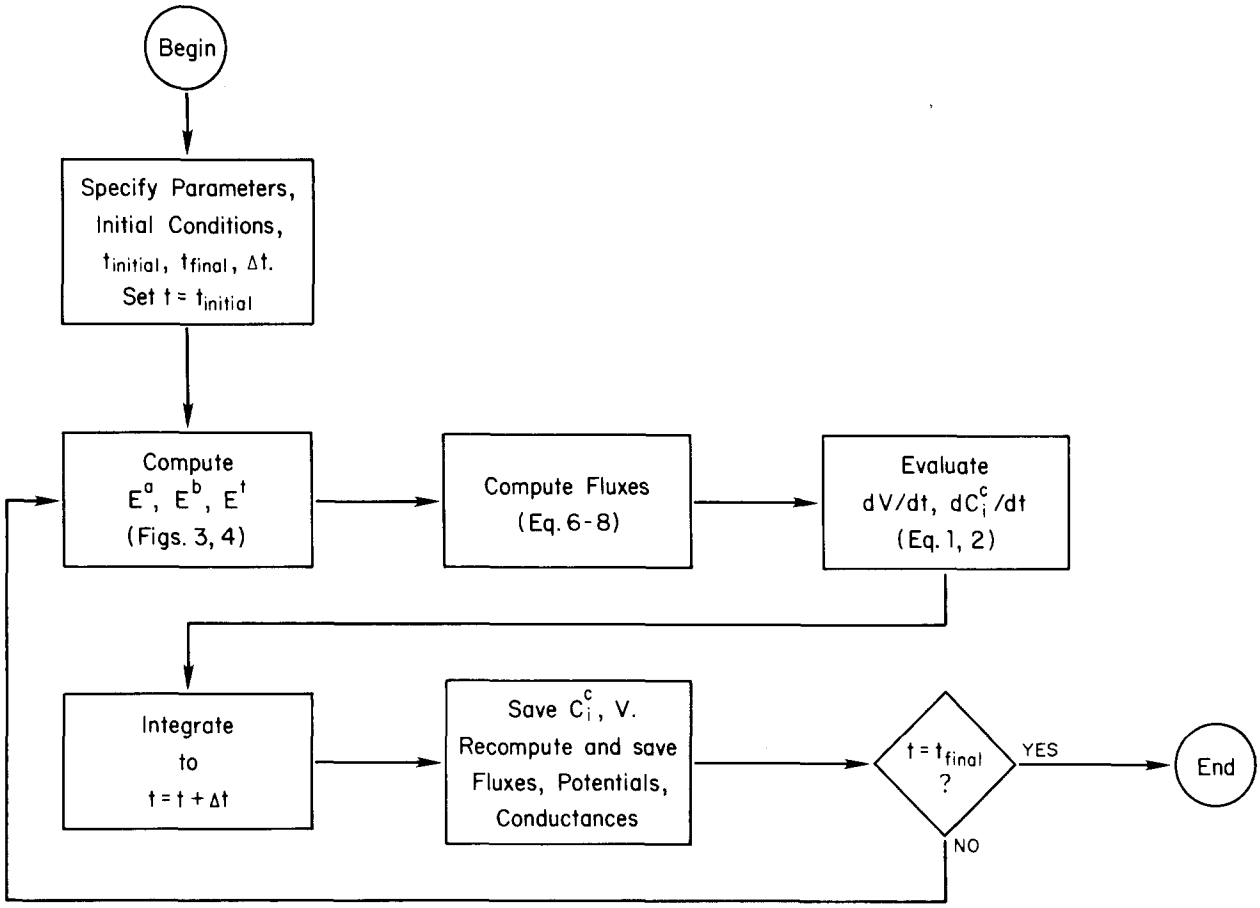

Fig. 2. Flow chart showing the overall computational scheme for evaluating the Na^+ model. Circles show entry and exit points; boxes show computations; diamonds show decisions and resulting branches in the flow of the overall computation. Consult the text for a detailed discussion of each step

$E^a + E^b$. In general, this problem cannot be solved analytically, and therefore a numerical procedure must be used. Our strategy is to (i) solve for I^a using the apical membrane fluxes at some E^a, (ii) solve for I^b using the basolateral membrane fluxes at $E^b = E^t - E^a$, (iii) compare I^a and I^b, and (iv) iteratively repeat this procedure changing E^a in a systematic way until $I^a = I^b$. This iterative procedure is accomplished using the Newton-Raphson algorithm (Acton, 1970, p. 51)[3] for finding the zero of a transcendental function. The computational steps are shown as a flow chart in Fig. 3, and are detailed as follows:

1. We start with an estimate of E^a, such as a portion of E^t, an equilibrium potential across the apical membrane for one or more of the permeant ions, or simply the value of E^a resulting from the previous step of the integration. This initial estimate need not be accurate since it will subsequently be refined by the algorithm.

2. We compute $E^b = E^t - E^a$.

3. Using the values of E^a and E^b, we then compute I^a and I^b (Eq. 3) using the flux equations (Eqs. 7 and 9).

4. We compare I^a and I^b and if they are equal to within 0.001%, then the computed membrane potentials are consistent with the requirement for cellular electroneutrality, and hence we proceed with the integration. Otherwise, we refine E^a using a Newton-Raphson step[4], and return to step 2.

This procedure results in rapid convergence to a solution usually in less than ten iterations.

Open-Circuit and Current-Clamp Case

Under current-clamp conditions, I^t is specified and held constant and the resulting transepithelial potential E^t is computed. The open-circuit case corresponds to the situation where $I^t = 0$.

[3] Available as subroutine ZREAL2 from the IMSL Library (International Mathematical and Statistical Libraries, Inc., Houston, Texas).

[4] The Newton-Raphson algorithm solves for U^a such that $f(U^a) = I^a - I^b = 0$, and this requires computation of df/dU^a. A finite-difference approximation of df/dU^a is used, which requires accurate computation of $f(U^a)$ for all values of U^a. A polynomial approximation for $z_i U^a/[1\text{-}\exp(z_i U^a)]$ must be used when evaluating the Goldman-Hodgkin-Katz flux equation at $|z_i U^a| < 0.1$ (*see* Dwight, 1961, p. 132). Similar care must also be taken when solving for U^t.

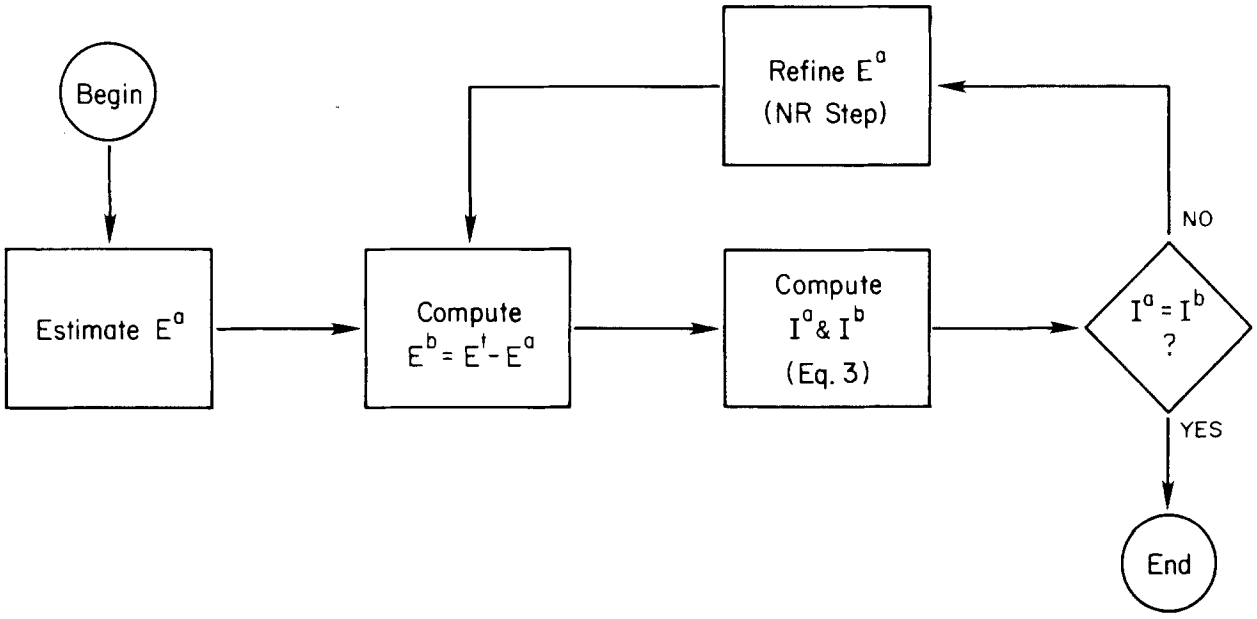

Fig. 3. Flow chart showing the numerical scheme for computing the membrane potentials under simulated voltage-clamp conditions. *See* Fig. 2 legend for description of the flow-chart symbols, and consult Methods for a detailed discussion of each step. NR denotes Newton-Raphson

In the case where the paracellular pathway has negligible ionic permeability (i.e., $P_i^j = 0$), as is the case in some tight epithelia, then $I^j = 0$ and $I^t = I^a = I^b$. The computation of E^a and E^b (and hence E^t) is straightforward and follows a similar procedure as described above. However, in the general case when $P_i^j \neq 0$, then the computation is complicated by the fact that a loop of current will flow across the transcellular pathway and back via the paracellular pathway. In addition to the cellular electroneutrality constraint of Eq. (4), maintenance of mucosal and serosal bath electroneutrality requires that $I^a + I^j = I^t$. In this case we must simultaneously determine two membrane potentials: E^t and either E^a or E^b.

Again, a numerical procedure must be used since analytical expressions are not available for the general case. In actuality, a nested Newton-Raphson procedure is used, where the outer procedure determines E^t, and the inner procedure is identical to the voltage-clamp case and determines E^a and E^b. The steps in the computation are shown as a flow chart in Fig. 4, and are detailed as follows:

1. An initial value for E^t is estimated using a method similar to that described above for the voltage-clamp case. Again, its actual value need not be accurate since it will subsequently be refined by the iterative procedure.

2. At this point, the epithelium can be considered for the moment to be voltage clamped at our current value of E^t, and hence we solve for E^a and E^b using the procedure described above. Recall that this calculates the transcellular current $I^a = I^b$.

3. I^j is computed using Eq. (12) and the current value of E^t.

4. We now compute $I^j + I^a$ and compare it to I^t. If they are equal to within 0.001%, then E^t, E^a and E^b are consistent with the requirements of electroneutrality, and we proceed with the integration. Otherwise, we refine E^t using a Newton-Raphson step and return to step 2.

Program Design and Computational Requirements

All computer programs were written in FORTRAN. The main program solves the general model, and it relies on three different subprograms to evaluate the specific flux equations for the apical, basolateral and junctional membranes, respectively. Changes to the flux equations, thereby changing the Na^+ model, require modifications of only the appropriate subprogram(s); the rest of the code remains unchanged. Six different solutes are specified, but this number is determined by an internal parameter that can be changed at will, thereby affecting all program units.

Computations were performed on PDP-11/23 and 11/34 computers (Digital Equipment Corp.). The model is readily adaptable to a general-purpose laboratory minicomputer possessing at least 64 Kbytes of main memory. Both computers possessed hardware for high-speed floating-point arithmetic. Under simulated open-circuit conditions, computation time was approximately one-third experimental time, requiring 300 sec of computer time to simulate 1000 sec of experimental time using 10-sec intervals. Simulated voltage-clamp conditions ran at twice this speed. Similar machines lacking floating-point hardware typically require six times more computer time. Hence, the time required to run a simulation is within the capabilities of a small laboratory computer.

During the computation, results were stored off-line and were subsequently printed in tabular form, or displayed graphically on a graphics terminal and/or digital plotter. The following variables were saved as a function of time: C_i^c, V, J_i^a, J_i^b, J_i^j, J_i^l, E^a, E^b, G^a, G^b and G^j. G^a, G^b and G^j (S) are the respective membrane conductances and were computed using a finite-difference method thereby providing an estimate of the slope conductances, as opposed to chord conductances. Namely, each of

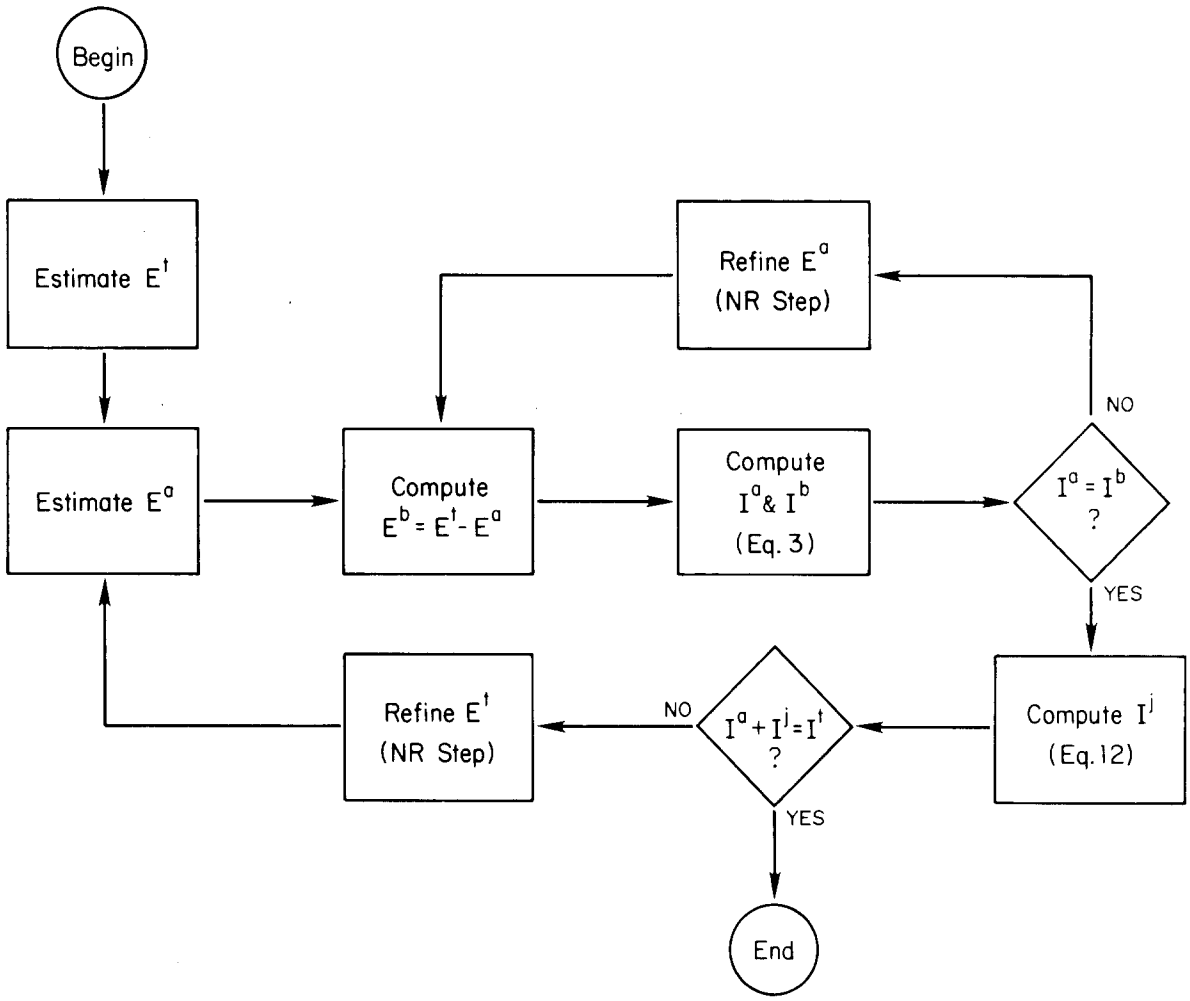

Fig. 4. Flow chart showing the numerical scheme for computing the membrane potentials under simulated current-clamp and open-circuit conditions; open-circuit occurs when I^t is set to zero. *See* Fig. 2 legend for description of the flow-chart symbols, and consult Methods for a detailed discussion of each step. NR denotes Newton-Raphson

the respective membrane potentials was incremented by a small voltage ΔE (typically 1 mV). The resulting change in membrane current ΔI was then computed from the change in the charge flux, and the conductance was calculated as $\Delta I/\Delta E$.

Verification of the Numerical Methods

The numerical procedure for computing the membrane potentials was verified by placing the Na^+ model under conditions that allow analytical computation of E^a and E^b. The simplest set of conditions that allow this are as follows: (i) simulation of open-circuit conditions ($I^t = 0$); (ii) only monovalent permeant ions ($|z_i| = 1$); (iii) completely impermeable junctions ($P_i^j = 0$); and (iv) zero sodium-pump current ($I_{max} = 0$). Under these conditions, I^a and I^b will be zero, and hence E^a and E^b can be computed analytically using the Goldman equation (Hodgkin & Katz, 1949). Simulation of these conditions produced calculated potentials that were indistinguishable from those obtained using the Goldman equation.

Results and Discussion

To evaluate the ability of the Na^+ model to simulate a transporting epithelium, the parameters and initial conditions listed in Table 1 were used. Most of these values correspond to measurements made in rabbit urinary bladder. This preparation was selected because it is a simple epithelium containing only one functional cell type, because it transports only sodium via an aldosterone-stimulated, amiloride-sensitive Na^+ transport system, and because nearly all membrane parameters have been measured and are available in the literature. For a discussion of Na^+ transport in this epithelium, consult Lewis and Diamond (1976).

In the simulation studies of rabbit urinary bladder with the Na^+ model, five solutes were considered: Na^+, K^+, Cl^-, X_1^- and X_2. The concentrations

Table 1. Parameters and initial conditions for rabbit urinary bladder

	Na^+	K^+	Cl^-	X_1^-	X_2
Permeabilities and initial concentrations:					
$C_i^{a,b}$ (mM)	104[a]	5.3[a]	102[a]	7.3	81.4
C_i^c (mM)	7[b]	72[a]	16[a]	63	142
P_i^a ($\times 10^{-9}$ cm/sec)	100[c]	50[c]	0[b]	0	0
P_i^b ($\times 10^{-9}$ cm/sec)	20[a]	463[a]	541[a]	0	0
P_i^j ($\times 10^{-9}$ cm/sec)	3[d]	3[d]	3[d]	0	0
$\sigma_i^{a,b}$	1	1	1	1	1

Hydraulic conductances[g]:

L_p^a[cm³/(dyne sec)]	L_p^b[cm³/(dyne sec)]
10^{-12}	10^{-11}

Pump kinetic parameters[b]:

K_{Na}(mM)	K_K(mM)	n_{Na}	n_K	I_{max}(μA/cm²)
14.2	2.3	3	2	5.61

Geometrical parameters:

A^a(cm²/cm² tissue)	A^b(cm²/cm² tissue)	V(cm³/cm² tissue)
1.8[e]	8.8[e]	0.001[f]

[a] From Lewis et al. (1978).
[b] From Lewis and Wills (1983).
[c] Absolute values are variable; listed values are typical for urinary bladder in that they produce P_{Na}^a/P_K^a equal to 2 and reasonable G^a and I^{sc} (*see* Lewis & Wills, 1981).
[d] Chosen to produce nonselective $G^j \sim 3$ μS/cm² (*see* Lewis & Wills, 1981).
[e] From Clausen, Lewis and Diamond (1979).
[f] Computed assuming 10 μm cuboidal cells.
[g] Values for urinary bladder unavailable; listed values are typical of other Na^+-transporting epithelia (*cf.* Welling, Welling & Ochs, 1983).

of X_3 (*see* Methods) were set to zero in the mucosal, serosal and intracellular compartments. X_1^- and X_2 represent a heterogeneous class of impermeant solutes that are osmotically active and may be charged, such as intracellular protein, ATP, phosphate, bicarbonate, sugars, etc. Because all these solutes are assumed to be impermeant, they can be lumped into two solutes, one charged and one uncharged. The concentrations of these solutes were chosen as follows. First, the Na^+, K^+ and Cl^- activities in the baths were set to measured values, as were the initial values for the intracellular activities of these ions. Second, the concentration of X_1^-, an impermeant monovalent anion, was chosen to balance electrical charge in the cell and baths. Finally, the concentration of X_2, a nonelectrolyte, was selected to produce solution osmolarities of 300 mOsm. The resulting initial concentrations are listed in Table 1.

The Steady-State Solution: Open-Circuit Case

The steady-state solution for the open-circuit case was obtained with the membrane permeabilities,

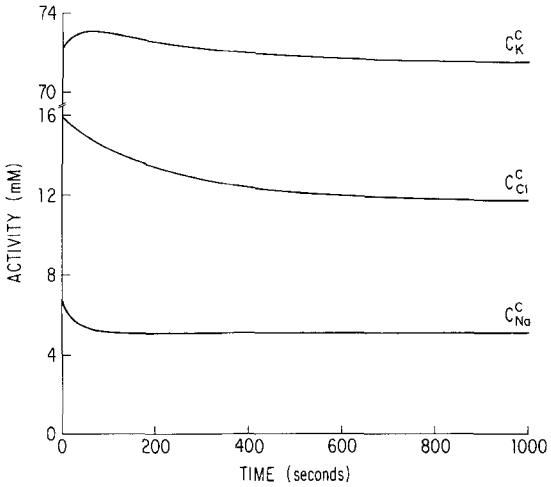

Fig. 5. Intracellular activities of Na^+, K^+ and Cl^- plotted as a function of time during integration of the Na^+ model to achieve a steady state under normal conditions. Transport parameters and initial ($t = 0$) conditions, representative of rabbit urinary bladder, are in Table 1. Final steady-state variable values (achieved after integration for 1000 sec) are in Table 2

pump kinetics, bathing solution composition and variable initial conditions $C_i^c(t = 0)$ and $V(t = 0)$ listed in Table 1. After initialization, the system of equations was then integrated over time until the intracellular solute activities stabilized to within the numerical accuracy of the program. Because the initial intracellular activities are equal to measured values, the extent to which the intracellular activities change from their initial values will be determined by (i) how well the Na^+ model describes transport in the tissue, and (ii) the degree of internal consistency of the set of transport parameters, values which were obtained under widely varying conditions with several different experimental methods. Hence, no attempts were made to fit the model predictions to measured values by arbitrarily adjusting the transport and geometrical parameters. This approach is fundamentally different than that used by Lew et al. (1979), where a steady-state solution was computed prior to integration of the model. Their method required an additional algorithm to *compute* the values of several parameters (notably P_{Na}^a and P_K^b) and initial concentrations (notably $C_K^{a,b,c}$ and C_{Na}^c) consistent with the remaining subset of specified parameters and initial concentrations.

The transition of the intracellular activities from their initial to their steady-state values is illustrated in Fig. 5. Table 2 compares the predicted steady-state values with experimentally measured values for rabbit urinary bladder. The model reached a steady state within 1000 sec, but it should be noted that the time required to attain a steady state is dependent on the surface area-to-volume ratio of

Table 2. Steady-state open-circuit values for rabbit urinary bladder

Variable	Model	Experimental	Reference
C^c_{Na} (mM)	5.1	5 to 7	Wills and Lewis (1978), Lewis and Wills (1983)
C^c_K (mM)	72	72	Lewis et al. (1978)
C^c_{Cl} (mM)	12	16	Lewis et al. (1978)
E^a (mV)	−17	−9.1 to 7.5	Lewis and Wills (1983)
E^b (mV)	−55	−53	Lewis and Wills (1983)
G^a (μS/cm^2)	26	~50	Lewis and Wills (1983)
G^b (μS/cm^2)	39	~125	Lewis and Wills (1981)
G^j (μS/cm^2)	2.4	<3	Lewis and Wills (1981)
α	7.5	~15	Lewis and Wills (1981)
I^{sc} (μA/cm^2)	2.3	0.8 to 2.5	Lewis and Wills (1983)
$V/V(t = 0)$	0.97	—	

Comparison of measured values with steady-state predictions of the Na^+ model. A steady state was achieved after integrating for 1000 sec using the parameters and initial conditions in Table 1. The membrane resistance ratio, as would be measured using a microelectrode, is defined as $\alpha = (G^b/G^a)(A^b/A^a)$.

the cells. The final steady-state variable values, however, are independent of absolute cell size as long as the ratio between apical and basolateral membrane areas remains constant. As seen in Table 2, the computed intracellular solute activities are in excellent agreement with experimental measurements. The slight decline in intracellular sodium resulted in a small transient rise in C^c_K because of the coupled basolateral membrane pump. The predicted steady-state value for C^c_{Cl} (12 mM) is lower than the value measured with Cl^--selective electrodes (16 mM), but this value is not corrected for the effects of competing ions, notably HCO_3^- (Lewis et al., 1978). Applying these corrections results in a measured value of C^c_{Cl} that is close to 12 mM (S.A. Lewis, *personal communication*).

This agreement between predicted and measured values of C^c_{Cl} is in contrast to the findings of Lew et al. (1979) in their Na^+-transport model of frog skin. When these investigators assumed only passive Cl^- transport across the apical and basolateral membranes, predicted values for C^c_{Cl} were several times lower than experimental measurements. Frog skin, as well as other epithelia, are known to possess additional chloride transport processes (e.g., NaCl cotransport, *see* Frizzell, Field & Schultz, 1979), which facilitate Cl^- entry into the cells, resulting in intracellular levels that are above electrochemical equilibrium. When these processes were included in their formulation, C^c_{Cl} attained levels that were comparable to experimental measurements. However, such mechanisms have not been observed in mammalian urinary bladder under normal conditions[5]. Hence, the agreement between our model predictions and experimental measurements is not surprising.

There are some differences between predicted and measured values of E^a, G^a and G^b (the low value for the resistance ratio α is a direct result of the low value of G^b). These discrepancies are not unexpected since the measured values were obtained using a wide variety of different techniques and represent mean values obtained from different preparations: $C^c_{Na,K,Cl}$ were measured using ion-selective microelectrodes; $A^{a,b}$ were measured by equivalent-circuit analysis of epithelial impedance; $P^b_{Na,K,Cl}$ were determined by analysis of bi-ionic potentials; $P^a_{Na,K,Cl}$ were inferred from measurements of apical membrane conductances; and $P^j_{Na,K,Cl}$ were inferred from resistance-ratio (α) measurements involving the application of conductance-altering antibiotics (for details of each of the experimental methods, consult the references specified in Table 1). In addition, G^a (and hence α) is known to be dependent on transport rate which is highly variable in urinary bladder. For these reasons, no further effort was made to obtain exact agreement between the model predictions and the experimental measurements, since this would have required arbitrary adjustment of several of the parameters (notably $P^a_{Na,K,Cl}$). We will therefore use the steady-state values in Table 2 as a starting point for further simulations of more complicated experimental protocols.

Transition from Open- to Short-Circuit Conditions

Figure 6 shows net Na^+ flux $J^{net}_{Na} = J^a_{Na} + J^j_{Na}$ and net K^+ flux $J^{net}_K = J^a_K + J^j_K$ during the transition from open-circuit to short-circuit (voltage clamp at $E^t = 0$) conditions. The model parameters are shown in Table 1, and prior to the transition, the model was at the steady state shown in Table 2. During open-circuit conditions, the epithelium reabsorbs Na^+ at a rate of 5.7 pmol/(sec cm^2) and secretes K^+ at a rate of −4.8 pmol/(sec cm^2). The transition to short-circuit conditions results in a transient increase in Na^+ reabsorption with a gradual decline over approximately 200 sec to a steady-state value of 23 pmol/(sec cm^2). K^+ secretion is nearly eliminated and reaches a steady-state value of −0.65 pmol/(sec cm^2).

Lewis and Diamond (1976) found that I^{sc} is entirely accounted for by a mucosal-to-serosal Na^+

[5] Ifshin, Johnson and Eaton (1983) have observed an apical NaCl cotransport process, but only under conditions of low pH in the mucosal bathing solution.

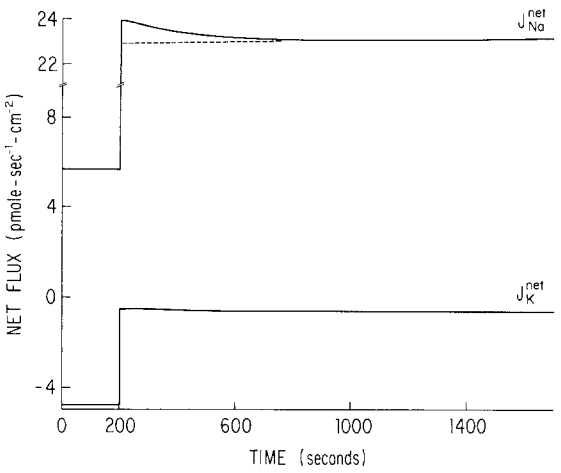

Fig. 6. Net Na^+ and K^+ fluxes under open-circuit conditions ($t <$ 200 sec), and following the transition to short-circuit conditions (voltage clamp at $E^t = 0$) at $t = 200$ sec. Transport parameters are in Table 1; the Na^+ model is initially at the steady state shown in Table 2. The dashed line in the upper Figure was drawn to emphasize the transient overshoot in J_{Na}^{net} following the transition to short-circuit conditions

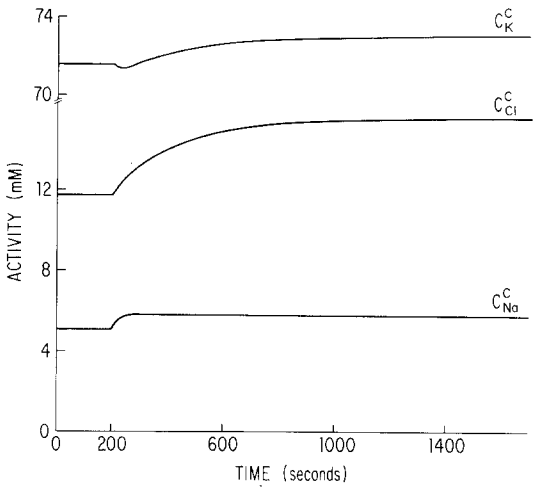

Fig. 7. Intracellular activities of Na^+, K^+ and Cl^- under open-circuit conditions ($t < 200$ sec), and following the transition to short-circuit conditions (voltage clamp at $E^t = 0$) at $t = 200$ sec. Transport parameters are in Table 1; the Na^+ model is initially at the steady state shown in Table 2

flux, as determined by measuring the transepithelial flux of $^{22}Na^+$. Under steady-state short-circuit conditions, I^{sc}/F is 22 pmol/(sec cm^2), in excellent agreement with the calculated net Na^+ flux. The almost negligible discrepancy in these two values is caused by the small residual K^+ secretion.

In order to interpret the changes in the net Na^+ and K^+ fluxes, it is necessary to know the changes in the electrochemical gradients across the cell membranes. This requires knowledge of changes in the intracellular solute activities during the open- to short-circuit transition, and these are shown in Fig. 7. The changes in J_{Na}^{net} and J_K^{net} are caused mostly by changes in E^a, since only small changes are observed in the intracellular ion activities (Fig. 7). Note that even though J_{Na}^{net} increased fourfold, C_{Na}^c exhibited an increase so small (from 5.1 to 5.8 mM) as to be undetectable using ion-selective electrodes. The increase in J_{Na}^{net} results from a large increase in the driving force for Na^+ entry across the apical membrane: the apical Na^+ equilibrium potential changes only slightly from -76 to -73 mV, while E^a dramatically increases from -17 to 47 mV during the transition from steady-state open- to short-circuit conditions. Similarly, the decrease in J_K^{net} is caused by E^a taking on a value closer to the apical K^+ equilibrium potential (66 mV during both steady-state open- and short-circuit conditions). Again, these same results are observed experimentally and are discussed in Lewis and Wills (1983).

The slow transient decay to a steady state observed in J_{Na}^{net} (Fig. 6) followed subtle rearrangements in intracellular solute activities after switching to the short-circuit condition. C_{Na}^c increased from 5.1 to 5.8 mM, C_{Cl}^c increased from 12 to 16 mM, and C_K^c increased from 72 to 73 mM. The increase in C_{Cl}^c was caused purely by the change in E^b ($= E^a$), since Cl^- is close to electrochemical equilibrium across the basolateral membrane, as has been observed experimentally (*see* Lewis et al., 1978). The change in C_K^c is biphasic and is caused by the simultaneous change in the basolateral K^+ electrochemical gradient and the pump rate. Since all permeant-solute activities increased, cell volume rose, but only by 2.9%. Even though the electrochemical gradients across the apical and basolateral membranes were changed significantly, thereby resulting in large changes in the ion fluxes, cell volume remained nearly constant since only a negligible change was observed in C_K^c (the most abundant permeant solute) and since the impermeant solutes X_1^- and X_2 are at high intracellular concentrations (*see* Table 1).

Sodium Pump Electrogenicity

The basolateral sodium pump is electrogenic in nature and results in a hyperpolarization of the basolateral membrane; it acts as a current source because of the nonunity Na^+-to-K^+ coupling ratio. Under normal conditions, the amplitude of the pump potential (<5 mV) is usually masked by the relatively large basolateral membrane potential (~50 mV).

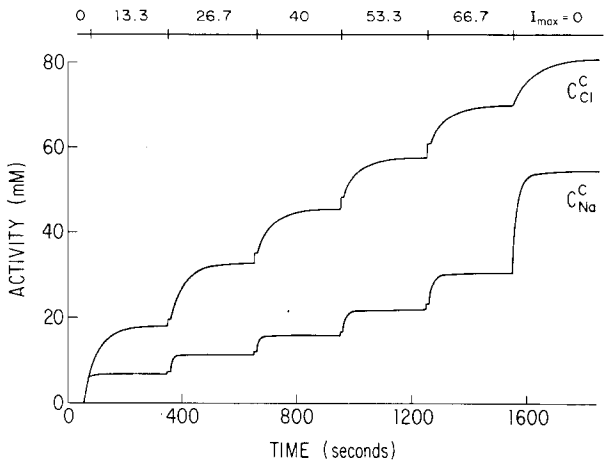

Fig. 8. Intracellular activities of Na^+ and Cl^- computed in a nystatin-treated preparation under open-circuit conditions. The values at the top of the Figure show bathing solution activities of Na^+ and Cl^- (in mM), resulting from stepwise additions of NaCl to both baths. At t = 1550 sec, the pump rate is set to zero, simulating the addition of ouabain to the serosal solution

Lewis et al. (1978) and Lewis and Wills (1981) devised an experimental protocol that allowed them to measure the pump potential directly, thereby permitting the study of pump kinetics and the determination of pump activity as a function of C^c_{Na}. To evaluate the Na^+ model further, this complicated experimental protocol was simulated for comparison with published results.

The experimental procedure was as follows. First, normal bathing solutions were replaced with solutions containing zero Na^+ and Cl^- with replacement by K_2SO_4. The polyene antibiotic nystatin was then added to the mucosal solution, which resulted in a 100-fold increase in the apical membrane permeability to monovalent ions (*see* Lewis et al., 1977), dissipated all membrane electrochemical gradients, and reduced E^t to zero. Subsequently, varying symmetrical amounts of NaCl (13.3, 26.7, 40, 53.3 and 66.7 mM) were added, first to the serosal solution and then to the mucosal solution. This resulted in a two-phase hyperpolarization in E^t. The rapid phase was caused by an apical membrane diffusion potential, and allowed calculation of C^c_{Na}. A slower phase was attributed to the pump potential resulting from the increase in pumping rate.

The results of the Na^+ model simulation of this experiment are shown in Figs. 8 and 9. The mucosal and serosal solutions were initialized to the following composition: $C^{a,b}_{Na} = C^{a,b}_{Cl} = 0$, $C^{a,b}_K = C^{a,b}_{X_1} =$ 109.3 mM, and $C^{a,b}_{X_2} = 81.4$ mM. The nystatin-induced apical membrane permeability is approximately three-to-one cation-to-anion selective (Lewis et al., 1977) and was simulated by setting $P^a_{Na,K} = 3 \times 10^{-5}$ cm/sec, and $P^a_{Cl} = 1 \times 10^{-5}$ cm/sec. The values of all additional parameters were left unchanged from those found in Table 1. A steady state was reached and resulted in E^t and C^c_{Na} equal to zero. The apical membrane conductance was 10 mS/cm^2, which is in close agreement with experimental measurements (Lewis et al., 1977).

The NaCl concentration was increased stepwise to the different concentrations noted above, by addition first to the serosal solution, followed by addition to the mucosal solution 10 sec later. This resulted in the stepwise increases in the intracellular activities seen in Fig. 8. C^c_{Na} stabilized at levels considerably lower than $C^{a,b}_{Na}$, as a result of the pump rate. The values agree well with those observed experimentally: the Na^+ model predicts activities of 6.9, 12, 16, 22 and 31 mM, resulting from the respective steps in bathing solution NaCl concentrations; the measured values were 7.9, 11, 15, 19 and 23 mM, respectively (*see* Lewis & Wills, 1983).

Figure 9 shows the resulting change in E^t after each sequential increase in NaCl and, for comparison, the measured results (inset). The agreement in the steady-state amplitudes of E^t between the Na^+ model and the measured results is good and somewhat surprising, since the experimental record was obtained from a single preparation, whereas the Na^+ model parameters are mean values from many different preparations. Clearly, the time course and the shape of the transitions illustrated in Fig. 9 differ between the Na^+ model and the experimental record. However, these differences are to be expected because changes in bathing solution composition are instantaneous when running the Na^+ model, but require approximately 30 sec experimentally (Lewis et al., 1978). In addition, unstirred-layer effects are ignored in the Na^+ model, but experimentally one estimates unstirred-layer thickness at approximately 300 μm. Both of these effects contribute to the slow response of the actual epithelium to changes in solution composition.

Inhibition of the Sodium Pump

To verify that the E^t response shown in Fig. 9 represents the pump potential, oubain was applied to the serosal bath at the end of the experiment to selectively inhibit pump activity. Experimentally, this manuever results in a decline in E^t towards zero, thereby confirming that most of the observed potential was due to the action of the pump. However, since C^c_{Na} and C^c_{Cl} never attained values equal to those in the bathing solutions, small but finite electrochemical gradients must exist across the basola-

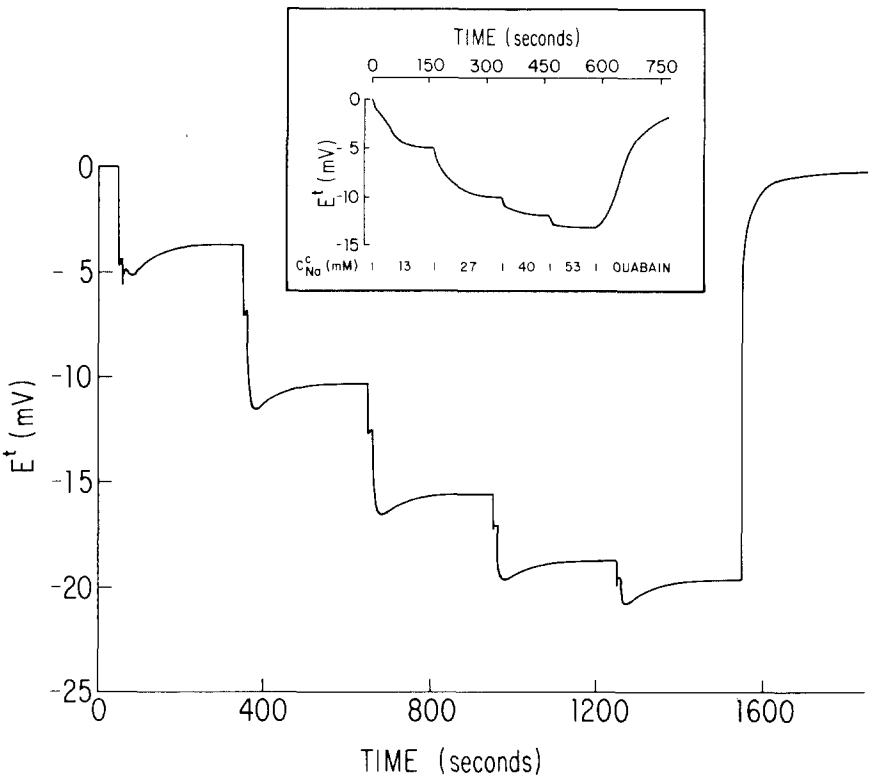

Fig. 9. Transepithelial potential E^t in a nystatin-treated preparation under open-circuit conditions. The changes in potential result from stepwise increases in the bathing solution activities of Na^+ and Cl^-; consult Fig. 8 for the time course of the changes in these activities. The main Figure shows the predictions of the Na^+ model, whereas the inset shows the experimentally observed response (redrawn from Lewis et al., 1978). At t = 1550 in the main Figure, the pump rate is set to zero, simulating the addition of ouabain to the serosal solution

teral membrane and would be expected to contribute to E^t. The action of the pump itself is also expected to add to these gradients. If the pump could be inhibited instantaneously, then the resulting immediate reduction in E^t could be attributed directly to the pump, whereas slower changes could be attributed to dissipation of the basolateral membrane electrochemical gradients.

Inhibition of the pump in the simulation was accomplished by setting $I_{max} = 0$. This resulted in an instantaneous reduction of E^t to −4.4 mV; further reduction of E^t to zero followed the subsequent changes in intracellular composition, as can be seen by comparing Figs. 8 and 9. Experimentally, the addition of ouabain resulted in a reduction of E^t to −1.5 mV within 180 sec (Fig. 9 inset); an instantaneous depolarization was not observed as a result of the time required for ouabain to cross the basolateral unstirred layer. Hence, pump inhibition and changes in intracellular composition most likely occur over similar time courses in the experimental preparation.

Finally, it is interesting to note that after inhibition of the pump, the Na^+ model predicts that the cell will swell by 11% before attaining a new steady state in which C^c_{Na} is lower and C^c_{Cl} is higher than their respective bathing solution activities. This expected result reflects the establishment of a Donnan equilibrium owing to the different intracellular versus extracellular concentrations of impermeant solutes.

Conclusions

By following the formalism outlined in this paper, dynamic, general models of epithelial transport can be derived easily. The resulting models can be termed general because the state equations and electroneutrality constraints are applicable to any epithelial structure. All that must be done to simulate a particular tissue is to supply a set of flux equations and boundary conditions appropriate for the epithelium of interest. These auxiliary equations may be simple algebraic expressions, or as complex as a probabilistic model of a membrane ionic channel. In any case, the differential equations that invoke mass conservation and electroneutrality would be the same.

Similarly, the numerical procedure developed for the calculation of transmembrane potentials can be termed general since it is independent of the mechanism of membrane ion transport. For those specific cases where the membrane potentials can be computed analytically, the procedure produces identical results. However, the procedure is flexible enough to permit the simulation of complex situations which cannot otherwise be solved using analytical techniques. Finally, the numerical procedure

is efficient enough to be implemented on a laboratory computer of modest capability.

The Na^+ model, which we developed primarily to evaluate the feasibility of the modeling strategy and numerical methods, showed a remarkable ability to reproduce experimental observations. This agreement demonstrates the adequacy of the basic concepts comprising the model to describe Na^+ transport in urinary bladder under the limited range of conditions we have considered. Moreover, because this agreement was obtained without fitting the model predictions to the experimental data, these results also indicate a high degree of internal consistency in the measured membrane transport parameters. This is a reassuring finding since these values were obtained from a number of different investigations, each designed to isolate specific processes in each of the different epithelial membranes.

We do not wish to imply that the agreement between the model and measurements indicates that this simple model represents the final word on Na^+ transport in mammalian urinary bladder. As discussed previously, several processes that are important determinants of epithelial function, notably P_i^a dependence on C_i^a, changes in P_i^a resulting from intracellular feedback, and changes in A^a resulting from fusion of cytoplasmic vesicles, were not included in the model. Under other experimental conditions, where these and other transport mechanisms come into play, we fully expect this model to fail. Indeed, much can be learned from analysis of a model's inability to reproduce experimental observations since this requires a critical re-examination of the hypotheses and data upon which the model is based.

Another potential use of this kind of model is in experimental design and retrospective data analysis. As an example, the generality of the basic model structure and our numerical methods allow a newly proposed transport mechanism to be included, and its potential impact on overall epithelial behavior to be examined. By contrasting the responses with and without the mechanism, experimental forcings can be designed that evoke measureable differences in behavior. Clearly, such efforts must be done with care and circumspection since the results of a simulation study are only as good as the assumptions and parameters that it uses. However, when properly used and carefully interpreted, such models can be powerful tools for the experimental investigator.

We with to thank Drs. S.A. Lewis and N.K. Wills for many helpful discussions. This work was supported by NIH grants AM 28074 to Dr. Clausen, and AM 26341 to Dr. Moore.

References

Acton, F.S. 1970. Numerical Methods that Work. p. 51. Harper and Row, New York

Carnahan, B., Luther, H.A., Wilkes, J.O. 1969. Applied Numerical Methods. Ch. 6. Wiley and Sons, New York

Civan, M.M., Bookman, R.J. 1982. Transepithelial Na^+ transport and the intracellular fluids: A computer study. *J. Membrane Biol.* **65:**63–80

Civan, M.M., Peterson-Yantorno, K., DiBona, D.R., Wilson, D.F., Erecińska, M. 1983. Bioenergetics of Na^+ transport across frog skin: Chemical and electrical measurements. *Am. J. Physiol.* **245:**F691–F700

Clausen, C., Lewis, S.A., Diamond, J.M. 1979. Impedance analysis of a tight epithelium using a distributed resistance model. *Biophys. J.* **26:**291–318

Dwight, H.B. 1961. Tables of Integrals and other Mathematical Data. p. 132. Macmillan, New York

Forte, T.M., Machen, T.E., Forte, J.G. 1977. Ultrastructural changes in oxyntic cells associated with secretory function: A membrane-recycling hypothesis. *Gastroenterology* **73:**941

Frizzell, R.A., Field, M., Schultz, S.G. 1979. Sodium-coupled chloride transport by epithelial tissues. *Am. J. Physiol.* **236:**F1–F8

Fuchs, W., Hviid Larsen, E., Lindemann, B. 1977. Current voltage curve of sodium channels and concentration dependence of sodium permeability in frog skin. *J. Physiol. (London)* **267:**137–166

Gluck, S., Cannon, C., Al-Awqati, Q. 1982. Exocytosis regulates urinary acidification in turtle bladder by rapid insertion of H^+ pumps into the luminal membrane. *Proc. Natl. Acad. Sci. USA* **79:**4327–4331

Hodgkin, A.L., Katz, B. 1949. The effect of sodium ions on the electrical activity of the giant axon of the squid. *J. Physiol. (London)* **108:**37–77

Hull, T.E., Enright, W.H., Jackson, K.R. 1976. User's guide for DVERK—A subroutine for solving non-stiff ODE's. TR No. 100, Dept. of Computer Science, University of Toronto

Ifshin, M.S., Johnson, K.E., Eaton, D.C. 1983. Acid pH and weak acids induce Na-Cl cotransport in the rabbit urinary bladder. *J. Membrane Biol.* **72:**151–164

Koefoed-Johnson, V., Ussing, H.H. 1958. The nature of the frog skin potential. *Acta Physiol. Scand.* **42:**298–308

Lew, V.L., Ferreira, H.G., Moura, T. 1979. The behaviour of transporting epithelial cells. I. Computer analysis of a basic model. *Proc. R. Soc. London B* **206:**53–83

Lewis, S.A., Moura, J.M. de 1982. Incorporation of cytoplasmic vesicles into apical membrane of mammalian urinary bladder. *Nature (London)* **297:**685–688

Lewis, S.A., Diamond, J.M. 1976. Na^+ transport by rabbit urinary bladder, a tight epithelium. *J. Membrane Biol.* **28:**1–40

Lewis, S.A., Eaton, D.C., Clausen, C., Diamond, J.M. 1977. Nystatin as a probe for investigating the electrical properties of a tight epithelium. *J. Gen. Physiol.* **70:**427–440

Lewis, S.A., Eaton, D.C., Diamond, J.M. 1976. The mechanism of Na^+ transport by rabbit urinary bladder. *J. Membrane Biol.* **28:**41–70

Lewis, S.A., Wills, N.K., Eaton, D.C. 1978. Basolateral membrane potential of a tight epithelium: Ionic diffusion and electrogenic pumps. *J. Membrane Biol.* **41:**117–148

Lewis, S.A., Wills, N.K. 1981. Interaction between apical and basolateral membranes during sodium transport across tight epithelia. *In:* Ion Transport by Epithelia. S.G. Schultz, editor. pp. 93–107. Raven, New York

Lewis, S.A., Wills, N.K. 1983. Apical membrane permeability and kinetic properties of the sodium pump in rabbit urinary bladder. *J. Physiol. (London)* **341:**169–184

Nelson, M.J., Blaustein, M.P. 1980. Properties of sodium pumps in internally perfused barnacle muscle fibers. *J. Gen. Physiol.* **75:**183–206

Schultz, S.G. 1980. Basic Principles of Membrane Transport. 144 pp. Cambridge University Press, New York

Thomson, S.M., Suzuki, Y., Schultz, S.G. 1981. Current-voltage properties of the active sodium transport pathway across rabbit colon. *In:* Ion Transport by Epithelia. S.G. Schulz, editor. pp. 47–59. Raven, New York

Turnheim, K., Frizzell, R.A., Schultz, S.G. 1978. Interaction between cell sodium and the amiloride-sensitive sodium entry step in rabbit colon. *J. Membrane Biol.* **39:**233–256

Wade, J.B., Stetson, D.L., Lewis, S.A. 1981. ADH action: Evidence for a membrane shuttle mechanism. *Ann. N.Y. Acad. Sci.* **372:**106–117

Welling, L.W., Welling, D.J., Ochs, T.J. 1983. Video measurement of basolateral membrane hydraulic conductivity in the proximal tubule. *Am. J. Physiol.* **245:**F123–F129

Wills, N.K., Lewis, S.A. 1978. Intracellular Na^+ activity as a function of Na^+ transport rate across a tight epithelium. *Biophys. J.* **30:**181–186

Received 27 February 1984; revised 15 May 1984